Solar energetic electron probes of magnetic cloud field line lengths

S. W. Kahler,[1] S. Krucker,[2] and A. Szabo[3]

Received 2 February 2010; revised 23 April 2010; accepted 7 June 2010; published 21 January 2011.

[1] Magnetic clouds (MCs) are large interplanetary coronal mass ejections of enhanced and low-variance fields with rotations indicative of magnetic flux ropes originally connected to the Sun. The MC flux rope models require field lines with larger pitch angles and longer lengths with increasing distance from the MC axis. While the models can provide good fits to the in situ solar wind observations, there have not been definitive observational tests of the global magnetic field geometry, particularly for the field line lengths. However, impulsive solar energetic ($E > 10$ keV) electron events occasionally occur within an MC, and the electron onsets can be used to infer *Le*, the magnetic field line lengths traveled by the electrons from the Sun to the points in the MC where the electron onsets occur. We selected 8 MCs in and near which 30 solar electron events were observed by the 3DP instrument on the Wind spacecraft. We compared the corresponding *Le* values with calculated model field line lengths to test two MC models. Some limitations on the technique are imposed by variations of the models and uncertainly about MC boundary locations. We found generally poor correlations between the computed electron path lengths and the model field line lengths. Only one value of *Le* inside an MC, that of 18 October 1995, exceeded 3.2 AU, indicating an absence of the long path lengths expected in the highly wound outer regions of MC models. We briefly consider the implications for MC models.

Citation: Kahler, S. W., S. Krucker, and A. Szabo (2011), Solar energetic electron probes of magnetic cloud field line lengths, *J. Geophys. Res.*, *116*, A01104, doi:10.1029/2010JA015328.

1. Introduction

[2] Magnetic clouds (MCs) are defined as interplanetary magnetic flux ropes with the following observational criteria [*Burlaga*, 1995]: (1) smooth rotations of the magnetic field direction of about 180° over about a day, (2) enhanced magnetic field strengths, and (3) low proton temperatures and low proton β. They compose about one quarter of all interplanetary CMEs (ICMEs) [*Cane and Richardson*, 2003]. Properties of MCs such as their types of rotation and their variations through the solar cycle have been extensively studied [*Wimmer-Schweingruber et al.*, 2006; *Forbes et al.*, 2006]. The magnetic field structure has been modeled as a locally cylindrically symmetric constant α force-free field in which B_r, the field component perpendicular to the rope axis, is 0, and the B_ϕ and B_z components are described by Bessel functions [*Burlaga*, 1995]. The well known cartoon introduced by *Burlaga et al.* [1990] and widely reproduced [*Burlaga*, 1995, Figure 6.5] shows schematically that the field lines are more highly wound and therefore longer in length with increasing distance from the flux rope axis. Whether the field lines connect back to the Sun as flux rope footpoints was left uncertain, although others have assumed extension of the flux rope structure to the Sun [e.g., *Farrugia et al.*, 1993; *Larson et al.*, 1997; *Zurbuchen and Richardson*, 2006].

[3] MC modeling efforts have become more sophisticated to take into account MC pressure gradients and dynamic expansions [*Russell and Mulligan*, 2003; *Forbes et al.*, 2006]. Multiple spacecraft fits to MCs based on observations with STEREO spacecraft separations on the order of the MC radius R_0 are now beginning and appear to confirm the basic flux rope model [*Liu et al.*, 2008; *Kilpua et al.*, 2009]. However, because all MC models have been developed using near-Earth observations [*Zurbuchen and Richardson*, 2006], independent techniques are needed to verify the model fits and to explore the large-scale magnetic structures connecting the local MC fields with solar fields.

1.1. Solar Energetic Particles as Probes of MC or ICME Magnetic Structures

[4] While the heat-flux electron BDEs are the standard signatures of closed magnetic fields in MCs [*Shodhan et al.*, 2000; *Larson et al.*, 1997] and ICMEs in general, attempts to use heat-flux pitch-angle distributions (PADs) to resolve a distinct population of BDEs from unidirectional periods have not been successful. Ratios of the ~350 eV electron flux parallel and antiparallel to the interplanetary magnetic field (IMF) to that perpendicular to the IMF yielded the expected statistical bimodal plot of unidirectional heat fluxes but no

[1]Space Vehicles Directorate, Air Force Research Laboratory, Hanscom Air Force Base, Massachusetts, USA.
[2]Space Sciences Laboratory, University of California, Berkeley, California, USA.
[3]Heliospheric Physics Laboratory, NASA Goddard Space Flight Center, Greenbelt, Maryland, USA.

0148-0227/11/2010JA015328

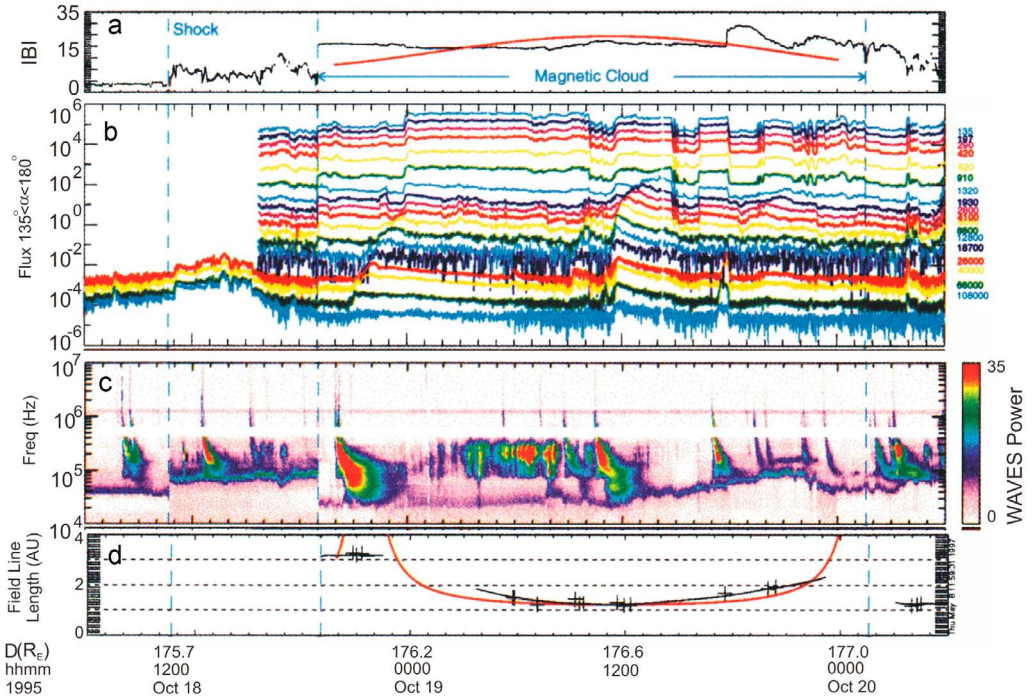

Figure 1. Composite panel of particles and fields measurements on the Wind spacecraft in the 18–20 October 1995 MC. (a) Observed and modeled interplanetary magnetic field of the MC 6. (b) The 3DP electron fluxes antiparallel to the IMF and (c) the WAVES 10 MHz to 10 kHz emission. (d) The continuous red line shows the computed model MC field line lengths L_{FC} and the black line is an eye fit to the cross symbol points calculated from the 3DP electron onset times. Each cross indicates one energy channel measurement; clusters of points indicate each electron event. The cluster of points at 2200 UT 18 October are often cited as confirmation of the extended field line length near the outer boundary of the MC. Reconstructed from *Larson et al.* [1997].

evidence of a separate BDE population [*Feuerstein et al.*, 2004] indicating closed magnetic topologies. *Owens et al.* [2009] modeled the behavior of the 272 eV electron strahl widths in MCs as a function of distance from the MC magnetic axis. They assumed the standard Lundquist fit to a constant-α force-free flux rope, self-similar expansion and kinematic distortion of the MC with heliocentric distance, and adiabatic focusing and pitch-angle scattering of the electrons. Their model strahl widths were broadest in the poloidal fields near the boundaries and narrowest at the more toroidal fields closest to the MC axes. Their superposed epoch profiles of 74 MC strahl widths showed some evidence for that shape, but the trend was much weaker than predicted by their model. Thus while the BDEs provide an intuitively satisfying signature of closed magnetic fields in ICMEs, our confidence in that interpretation is not secure.

[5] Perhaps the optimum energetic particle population for probing ICME or MC structures are solar energetic (≥10 keV) electron events. $E > 40$ keV electron events have been reported in four ICMEs out to 5.4 AU on the Ulysses spacecraft [*Malandraki et al.*, 2000, 2001], indicating continued solar magnetic connection well beyond 1 AU and including one ICME extending to 4.1 AU well south of the ecliptic at 43°S heliograph latitude. Observed electron BDEs in the ICMEs indicated possible closed loops or reflection from magnetic mirrors formed beyond the spacecraft. In the case of closed loops the BDEs could arise from electron injections at the second solar footpoint or reflection from the converging fields above that footpoint [*Richardson*, 1997], even after that footpoint has undergone interchange reconnection [*Crooker et al.*, 2002] in the corona to become an open loop. As with the Ulysses ICMEs, $E > 40$ keV electron observations in two ICMEs in October/November 2003 on the ACE spacecraft [*Malandraki et al.*, 2005] showed extensive periods of both unidirectional and BDE flows suggesting complex magnetic geometries, with the origins of the BDEs uncertain.

1.2. Solar $E \geq 10$ keV Electrons as Probes of MC Field Lines

[6] The work cited above has focused on establishing MC or ICME field line connectivity to the Sun or the open versus closed field line topology. Because their small gyroradii ($\leq 10^2$ km in a 10 γ field) constrain the electrons to follow closely the field lines from Sun to 1 AU, solar energetic electron events may allow us to measure field line lengths and provide more definitive tests of MC model fields. The solar injection times are usually defined by associated type III radio bursts, and the 1 AU onset times of essentially scatter-free electrons yield the lengths to 1 AU of the MC field lines traversed by the electrons.

[7] Multiple energetic electron injections observed in an MC on 18–20 October 1995 allowed *Larson et al.* [1997] to validate quantitatively MC model field line lengths from the Sun to 1 AU (Figure 1). Their result is accepted [e.g.,

Table 1. Comparison of Measured and Calculated Field Line Lengths[a]

Date[b]	Type III (UT)	L_L (AU)	L_{FC} (AU)	*Le* (AU)	Data Points	D (AU)
			MC 6, $Q_0 = 1$			
18 Oct 1995	1956	2.3–5.1	2.0–>5	3.3–4.0	9	3.30
19 Oct 1995	0518	1.5	1.4	1.5–1.7	3	1.06
19 Oct 1995	0846	1.4	1.4	1.2–1.6	6	1.33
19 Oct 1995	1028	1.4	1.4	1.1–2.3	10	1.65
19 Oct 1995	1657	1.9	1.6	1.7–2.2	4	1.45
19 Oct 1995	2156	>5	>5	2.1–2.4	2	0.80
20 Oct 1995*	0550	1.2	1.2	1.0–2.4	8	0.55
			MC 21, $Q_0 = 3$			
17 Sep 1997	2359	>10	1.4	1.2–2.8	9	1.32
18 Sep 1997	1606	3.1	3.0	2.6–3.2	4	1.69
18 Sep 1997	1709	3.0	2.8	2.7–3.1	4	2.05
18 Sep 1997	1951	2.6	2.1	1.8–2.1	4	1.33
20 Sep 1997	0316	5.6	2.3	2.1–2.8	4	1.33
			MC 32, $Q_0 = 3$			
2 May 1998	1338	>10	4.1–7.6	1.0–1.7	14	1.18
			MC 54, $Q_0 = 2$			
6 Nov 2000*	1628	1.2	1.2	1.6–2.3	3	0.52
7 Nov 2000	0008	3.2–6.0	1.5	1.1–1.6	13	1.08
7 Nov 2000	1540	4.0–6.0	3.1–5.0	1.2–2.1	5	0.98
7 Nov 2000*	1829	1.2	1.2	3.6–4.5	3	3.53
7 Nov 2000*	2013	1.2	1.2	3.3–4.3	3	1.55
7 Nov 2000*	2223	1.2	1.2	2.5–2.8	4	2.17
			MC 61, $Q_0 = 2$			
10 Jul 2001	2253	2.9–3.8	1.8–2.3	1.5–2.5	7	1.41
12 Jul 2001	0111	3.8–4.6	2.1–3.2	2.7–3.6	4	2.05
			MC 72.2, $Q_0 = 3$			
1 Oct 2002	0912	2.5–>10	>10	1.7–2.7	11	1.57
			MC 80, $Q_0 = 2$			
24 Jul 2004	1843	2.0	1.4	1.3–1.5	9	1.14
25 Jul 2004	1200	>5	2.4–3.3	2.4–3.3	5	2.27
25 Jul 2004*	1336	1.2	1.2	0.9–1.3	3	1.72
			MC 81, $Q_0 = 1$			
29 Aug 2004*	0209	1.2	1.2	1.3–2.4	9	1.38
30 Aug 2004	0309	1.5	1.4	1.9–3.0	4	0.54
30 Aug 2004	1613	2.4–3.8	1.7–2.0	3.0–3.4	7	3.01
30 Aug 2004	1809	4.1–5.0	2.1	2.7–3.4	4	3.31
31 Aug 2004*	1406	1.2	1.2	1.4–2.1	11	0.95

[a] Q_0 = 1, 2, and 3 for good, fair, and poor fit, respectively.
[b] An asterisk indicates event outside the MC.

Richardson, 1997; *Wimmer-Schweingruber et al.*, 2006; *Linton and Moldwin*, 2009] as both a confirmation of the technique and support for twisted flux rope models. The technique is a scientific objective of the current STEREO In situ Measurements of Particles And CME Transients (IMPACT) investigation [*Lin et al.*, 2008; *Luhmann et al.*, 2008].

[8] Despite its apparent success, however, this technique has not been applied to other MCs. Furthermore, except for the inferred ≥3 AU travel path of the first electron event of Figure 1, the subsequent inferred path lengths appear consistent with either the MC model or with a ~1.2 AU spiral field line length. There is clearly a need for further testing of MC models, particularly in the outer portions of MCs where the tightly wound field lines should result in long (≥3 AU) path lengths. To accomplish this comparison we must find MCs with suitable cases of solar electron events, calculate the model field line lengths, and then compare the model lengths with those inferred from the electron onsets.

2. Data Analysis

2.1. Electron Event Selection and Analysis

[9] For a comprehensive and consistent MC list we used Magnetic Cloud Table 2, maintained at http://lepmfi.gsfc.nasa.gov/mfi/mag_cloud_S1.html, where the numbered 1–100 MC start and stop times and model parameter fits [*Lepping et al.*, 1990, 2006] are given for the period 1995–2007. The MC parameters are derived from a constant-α, cylindrically symmetric MC model using the Lundquist solution and are based on observations with the Magnetic Field Investigation (MFI) dual magnetometers on the Wind spacecraft [*Lepping et al.*, 1995]. The MC time intervals were compared with lists of impulsive $E > 30$ keV electron events

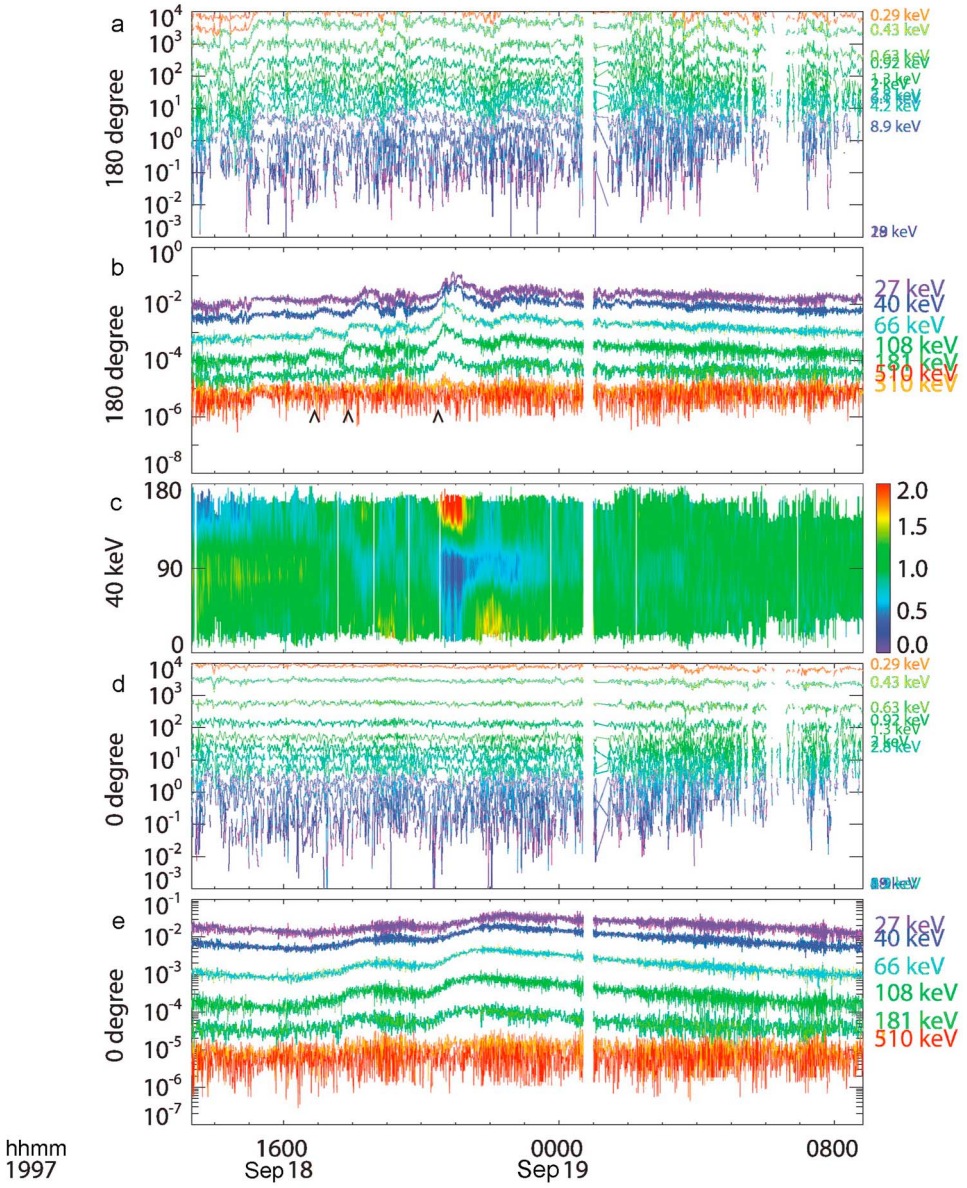

Figure 2. The 3DP electron fluxes for three electron events of MC 21. (a, b) The 0.3–28 keV channels of the EESA and the 27–510 keV channels of the SST aligned antiparallel to the local IMF. (c) The normalized pitch-angle distribution of the 40 keV electrons and (d, e) the EESA and SST electron fluxes parallel to the local magnetic field. Event onsets occurred at ~1650 UT, 1800 UT, and 2015 UT (arrows).

detected with the Wind 3DP instrument [*Krucker et al.*, 1999] to select those events occurring within or on the boundaries of the MCs. We found a total of 18 MCs within which 32 3DP electron event onsets occurred. Six MCs were associated with multiple (2 to 5) electron events. For this investigation we have examined 22 electron events in 8 MCs, listed by their MC number and quality of fit Q_0 in Table 1. Those MCs were selected for occurrence of multiple electron events and for electron event locations near the MC boundaries, which provide the best tests of field line lengths, as discussed below. As tests of the electron travel distances outside the MCs we included eight more electron events occurring within 18 h of the MC boundaries for a total of 30 electron events.

[10] For each electron event the onset times in each channel of the 3DP electrostatic analyzer (EESA) and/or solid state telescope (SST) where those onsets were sufficiently clear were determined using the procedure described by *Krucker et al.* [1999]. To determine the electron solar release time (SRT), we subtracted the 8.3-min Sun-Earth travel time of light from the peak time of the associated preceding WAVES type III radio burst at ~14 MHz, given in column 2 of Table 1. The travel distance *Le* was calculated for each energy by multiplying the electron average speed, using the geometric mean energy of each 3DP channel, by the time interval from SRT to onset at Wind. Figure 2 shows a stack plot of the 3DP electron fluxes during three events of MC 21, and Figure 3

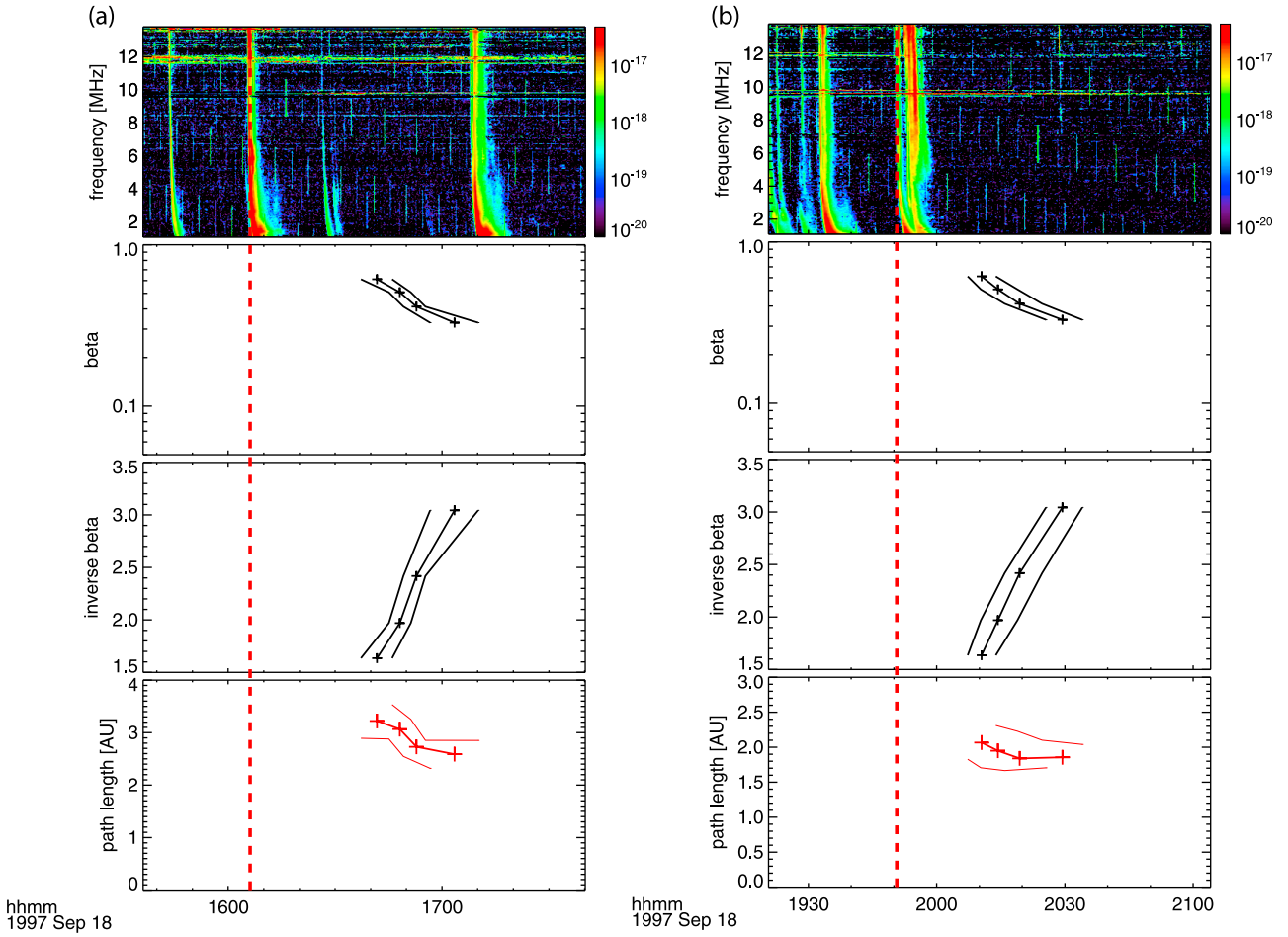

Figure 3. Electron onset plots for two of the electron events of Figure 2. Composites (from top) show 1–14 MHz WAVES data showing the associated type III burst with the vertical dashed line showing the burst onset, the β and inverse-β values for each energy onset time, and the inferred travel distances *Le* for each electron energy. Each data point corresponds to a channel in the 3DP detector and uncertainties are shown by the lines above and below the data points.

shows the WAVES plot and the $\beta = v/c$, inverse β, and inferred path length for each energy channel for two of the three events. In column 5 of Table 1 we give the approximate range of the path lengths *Le* for each event based on both the onset timing uncertainties of each energy channel, as indicated in Figures 3a and 3b, and the differences among those channels. The number of usable channels is given for each event in column 6 of Table 1. In general, the more channels used, the better the *Le* determination.

[11] If the MC is a flux rope connected to the Sun at both ends, it is possible that the energetic electrons might arrive from the longer leg [*Richardson and Cane*, 1996; *Richardson*, 1997], contrary to the assumption we make in the next section about the field line lengths. We have checked this possibility by confirming that the initial electron flow directions (parallel or antiparallel to the IMF) match those of the heat-flux electrons in all events excepting several cases in which the heat-flux BDEs precluded a clear dominant flow direction.

[12] This technique of inferring particle travel path lengths based on onset times in individual energy channels was also used by *Larson et al.* [1997], as shown in Figure 1d. Although subject to uncertainties, the popular alternative technique is to use the slopes of the inverse-β plots [*Kahler and Ragot*, 2006] directly to yield the electron travel distances, and we give those distances *D*, determined by eye fits to the inverse beta plots, in column 7 of Table 1. In general, $D < Le$ and is often unphysical, i.e., $D \leq 1.2$ AU. The individual channels used here are preferred to the inverse-β technique.

[13] A critical assumption of our analysis and that of *Larson et al.* [1997] is that the solar electron injections occurred at the times of type III bursts. This assumption is contrary to the finding of electron injection delays from the type III bursts by ~5–20 min [*Haggerty and Roelof*, 2002; *Haggerty et al.*, 2003]. That result, however, is based on an assumed 1.2 AU electron travel distance for beamed scatter-free electrons and remains controversial [*Kahler*, 2007]. Recent work to calculate model IMF lengths to 1 AU resulting from their extension by solar wind turbulence shows increases of simple spiral lengths by factors of ~1.3–1.6 [*Ragot*, 2006; *Ragot and Kahler*, 2008], which could account for ~6–12 min, or nearly all of the calculated electron injection delays. All but one of our *Le* values

(Table 1 and Figures 7 and 8) exceed 1.2 AU, in agreement with our assumed type III burst injections, and would be inconsistent with much shorter travel distances based on assumed injection delays of ~10 min.

2.2. Magnetic Field Line Length Calculations

[14] To compare the electron travel distances *Le* with the model field line lengths, we first let R_0 be the radius of the cylindrical cross section of the MC at 1 AU and let r be the distance from the axis. Thus r/R_0 is the dimensionless distance from the cloud axis. On the basis of CME coronagraph images we estimate the Sun-to-Sun length of the axial magnetic field line that reaches 1 AU at its most distant point to be 2.7 AU and have chosen a range of axial field line lengths L_0 from the spacecraft to the Sun as 1.35 ± 0.25 AU. Outside of the MCs a constant 1.2 AU Parker field line length is used. We use two methods to calculate the MC field line lengths. First, we use the traditional Lundquist solution [*Burlaga*, 1995; *Lepping et al.*, 2003, 2006] for which the length L_L of any field line from the Sun can be computed assuming a two-dimensional topology, characteristic of force-free flux ropes with no field components perpendicular to the rope axis. L_L can be expressed in terms of the axial and tangential components of the MC magnetic field, which are orthogonal to each other:

$$L_L = \int_0^{L_0} \left[1 + \left(\frac{J_1(\alpha r/R_0)}{J_0(\alpha r/R_0)} \right)^2 \right]^{1/2} dl \,, \qquad (1)$$

where J_0 and J_1 are Bessel functions, dl is an infinitesimal line segment along the axial field line, and α is a dimensionless constant usually set to the value of 2.4. The term under the square root is independent of dl and can be removed from the integral, thus making the integral trivial and yielding the length L_L of the axial uncoiled field line [*Farrugia et al.*, 1993]. That is, the MC field line length at any distance r from the axis of symmetry can be expressed as a function of the central field line length L_0. Note that this result is independent of the variation of R_0 as a function of ρ, the distance from the Sun. Using the 1 AU MC fits [*Lepping et al.*, 2006] for the timing and geometry, L_L at any point inside the MC can be estimated and compared to particle observations as shown for MCs 21 and 81 in the bottom panels of Figures 4 and 5. A similar plot for MC 54, which includes the electron events of Figure 3, is shown in the work of *Kahler et al.* [2009].

[15] Our second computational method uses magnetic flux conservation, which demands that the axial field component varies as $1/\rho^2$. On the other hand, current conservation in the cylindrically symmetric topology of a MC demands that the tangential component B_T vary as $1/\rho$. Since the Lundquist solution has only one free variable, the axial field strength B_0, at least one of these conservation laws is violated. It is, however, possible to maintain magnetic flux and current conservation and reformulate a field line length computation L_{FC}. Somewhat arbitrarily, one can model the radius of the circular magnetic cloud cross section as a function of the distance from the Sun along the cloud axis l as

$$R(l) = R_0 \sin\left(\frac{\pi}{2} \frac{l}{L_0} \right) . \qquad (2)$$

This simple Flux Conservation model, used by *Larson et al.* [1997], basically states that the cloud cross section radius $R(l)$ (minor radius) approaches zero at the two ends (near the Sun) and is maximum at the furthest point (1 AU). The advantage of the model is that it has only two free parameters: R_0, the minor radius at 1 AU, obtained from fits to the in situ measurements, and L_0, discussed above. Then using the ρ dependence of the magnetic field components derived above from the conservation principles, the field line length integral from above, and the simple cloud cross section model, we get

$$L_{FC}(r, L_0) = \int_0^{L_0} \left[1 + \left(\frac{B_T(r, L_0)}{B_A(r, L_0)} \sin\left(\frac{\pi}{2} \frac{l}{L_0} \right) \right)^2 \right]^{1/2} dl, \qquad (3)$$

where only the sin term has any l dependence. All other terms are constants that can be determined from 1 AU measurements. Note that this formulation does not assume or require an exact Lundquist Bessel function for the magnetic field at any location. The requirements of this model are that the MC still has approximate cylindrical symmetry; thus its cross section can be described with a minor radius R_0, and one can still define a dimensionless distance from the axis r/R_0. This is why in equation (3), we replaced the Bessel functions with the 1 AU field components. Though we no longer require a pure Lundquist solution, we still assume that the *Lepping et al.* [2006] flux rope fits give a reasonable estimate for the size, orientation, and impact parameter (the minimum r/R_0) of the MCs. At this point, we could take the actual measured magnetic field vectors at 1 AU and express them in MC coordinates. However, commonly superimposed on the MC fields are significant wave and other local features that do not represent global topological features. Therefore we use the smooth, fitted model field configurations generated by the *Lepping et al.* [2006] Lundquist solutions, which are also over-plotted on the data in Figures 4 and 5 (top).

[16] It also should be noted, as discussed at length by *Lepping et al.* [2006], that these fitted field profiles are allowed to go past the nominal boundaries of the ideal Lundquist flux ropes, leading to the reversal of the axial component. This does not adversely impact our conservation model as its input is simply the observed field line components. On the other hand, this was not allowed by our previous Lundquist formulation that assumed a pure Bessel function formulation of the MCs. We used equation (3) to evaluate numerically L_{FC} for each MC as shown in the examples of Figures 4 and 5, where they are compared with L_L and the values of *Le* from the electron events. The calculated L_L and L_{FC} values are given in the third and fourth columns of Table 1. When the values are changing rapidly over the onset times of the 3DP electron events, we give the estimated value range. Otherwise we assume an uncertainty of ±20% in L_L and L_{FC} scaled from our uncertainty in the above estimate of L_0. A detailed analysis of how the MC model parameters vary with magnetic field noise has been given by *Lepping et al.* [2003].

[17] The comparisons of the model field line lengths in Figures 4 and 5 reveal two important points. First, the two models differ little from the assumed axial lengths, taken here as 1.35 AU, across a broad range closest to the MC axis. The field line length differences increase as the MC boundary is approached, so the electron event test cases best for dis-

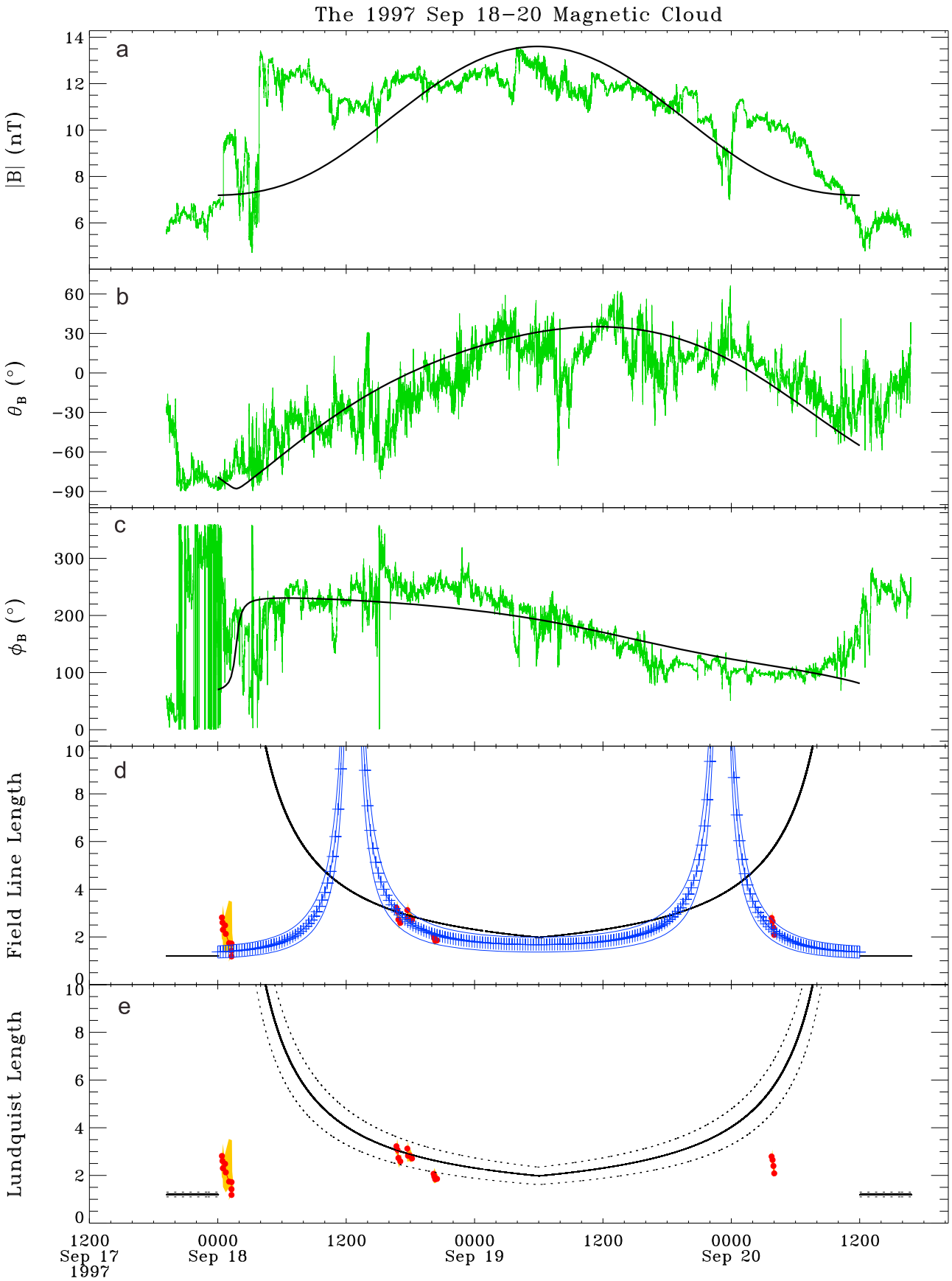
The 1997 Sep 18–20 Magnetic Cloud
a
|B| (nT)
b
θB (°)
c
φB (°)
d
Field Line Length
e
Lundquist Length
1200 Sep 17 1997
0000 Sep 18
1200
0000 Sep 19
1200
0000 Sep 20
1200

Figure 4

criminating either between models or between the MC interiors and exteriors will be those closest to the MC boundaries. Second, for some MCs the Flux Conservation model requires the reversal of flux sign discussed above and therefore of field direction in the outer region of the assumed MC interval [*Lepping et al.*, 2006]. In contrast, the Lundquist model we used requires orthogonal fields and the longest L_L at the MC boundary. This is evident in MC 21 (Figure 4) for which that model fit results in field lines orthogonal to the axis at $r/R_0 = 0.57$ and field lines roughly antiparallel to the axis field at $0.8 < r/R_0 < 1.0$. Note that the field line lengths calculated for MC 6 by *Larson et al.* [1997] show this effect on 18 October (Figure 1).

2.3. Alternative MC Boundary Determinations

[18] Our eight MCs are selected from the widely used list of *Lepping et al.* [2006], but other authors have treated some of those MCs with different assumptions about the boundary locations, which we summarize in Table 2. Columns 2 and 3 give the MC onset and end times from the MFI list which we use and the times from the more comprehensive list of ICMEs maintained [*Cane and Richardson*, 2003] at http://www.ssg.sr.unh.edu/mag/ace/ACElists/ICMEtable.html, as well as those of *Huttunen et al.* [2005] and *Jian et al.* [2006]. The agreement is best for MC 6 (the range of the onset times is 1 h and for the end times 0 h) and worst for MC 61 (the onset and end time ranges are 38 and 10 h). The median range for both boundaries is only 2–4 h. MC models based on times from alternative MC lists would not only yield field line lengths different from our calculations but even change a few 3DP electron events from outside to inside an MC or vice versa as noted in the last column of Table 2. In addition to the differences among MC models, the lack of agreement on MC boundaries is another mitigating factor in our confrontation of MC flux rope models with the energetic electron events.

3. Results

[19] The basic result of this work is shown in Figures 6 and 7, where we compare the calculated model field line lengths L_L and L_{FC} versus the electron path lengths *Le* of the 30 events of Table 1. For the Lundquist model (Figure 6) the agreement is generally poor. The correlation coefficient r = 0.08 is not significant. Eight of the 10 best test cases of $L_L > 4$ AU matched values of $Le < 2.5$ AU. For the Flux Conservation model (Figure 7) the agreement may appear slightly better because that model does not predict so many cases of large path lengths as the Lundquist model does. However, the correlation coefficient r = 0.04 for the Flux Conservation model is also not significant.

[20] The arrows in Figures 6 and 7 indicate the data point corresponding to the well known first electron event of MC 6 on 18 October 1995 shown in Figure 1. Its location near the MC boundary and its field line length of $Le \sim 3.2$ AU, compared to the $Le < 2$ AU lengths near the MC center are well noted, as discussed in section 1.2. Outstanding among our 3DP electron events, that point indicates excellent agreement of *Le* with both model values. Our broader view of additional MC electron events, however, contrasts that data point with the overall poor agreement of *Le* with the model values.

[21] If we accept that the models may not provide accurate field line lengths, we can still ask whether *Le* values show expected trends of larger values close to MC boundaries and smaller values near MC centers and outside the MCs. In Figure 8 we show a superposed epoch plot of values of *Le* relative to the normalized MC boundaries, whose durations ranged from 13 to 60 hours, indicated by the dashed lines at 0 and 1.0. The uncertainties in boundary locations reflect the range of onset times of the 3DP electron channels for each event. We expect that a few examples will indicate the longest lengths present in MCs, but the two largest *Le* values lie outside MCs. Excepting the 18 October 1995 case discussed above, we found no examples of 3DP electron events with $Le > 3.2$ AU inside any of the eight MCs of our study. The values of the eight *Le* points outside the MCs, used to contrast field line lengths outside MCs with those inside MCs, are not distinguished from the 22 points inside the MCs. We also indicate those events that other studies (Table 2) would have moved across the *Lepping et al.* [2006] MC boundaries.

[22] Finally, we can do a simple qualitative consistency check of the trends with time of the *Le* values for each energy channel within each 3DP event. The dispersion of the onset times, as illustrated in Figure 3, means that each energy onset samples a slightly different part of the MC. If the model field line lengths are increasing (decreasing) during the times of electron onsets, we expect to see the derived *Le* values increase (decrease) as well. Outside the MC the values of *Le* should be relatively flat within each event. The classification of the trends is somewhat subjective and sometimes the two models show opposite trends, but our result is 17 cases of trends in the presumed wrong direction, 10 in the right direction, and three ambiguous. Thus this simple test of trends of onset times does not support the MC models.

4. Discussion

4.1. Comparing the MC Models

[23] We have confirmed the good agreement of the electron path lengths with those of the flux conservation model for MC 6 found by *Larson et al.* [1997] and extended those comparisons to seven additional MCs, but we find the electron path lengths to be uncorrelated with the model field line lengths for the combined eight MCs. The 3DP electron path lengths were compared with the calculations from the Lundquist model and a magnetic Flux Conservation model

Figure 4. (a–c) Lundquist model fits to the IMF intensities and directions of MC 21 of Table 1. (d, e) The calculated Lundquist (dark solid line in Figures 4d and 4e) field line lengths L_L in units of AU as functions of time through the MC. The flat profiles outside the MC are an assumed nominal spiral field of 1.2 AU. Figure 4d shows the superposed flux conservation field line lengths L_{FC}. Dashed lines in Figure 4e and thin solid lines in Figure 4d indicate an assumed range of uncertainties based on the axial length $L_0 = 1.35 \pm 0.25$ AU. *Le* values from the electron onsets are indicated; each group of points corresponds to different energies of a single electron event.

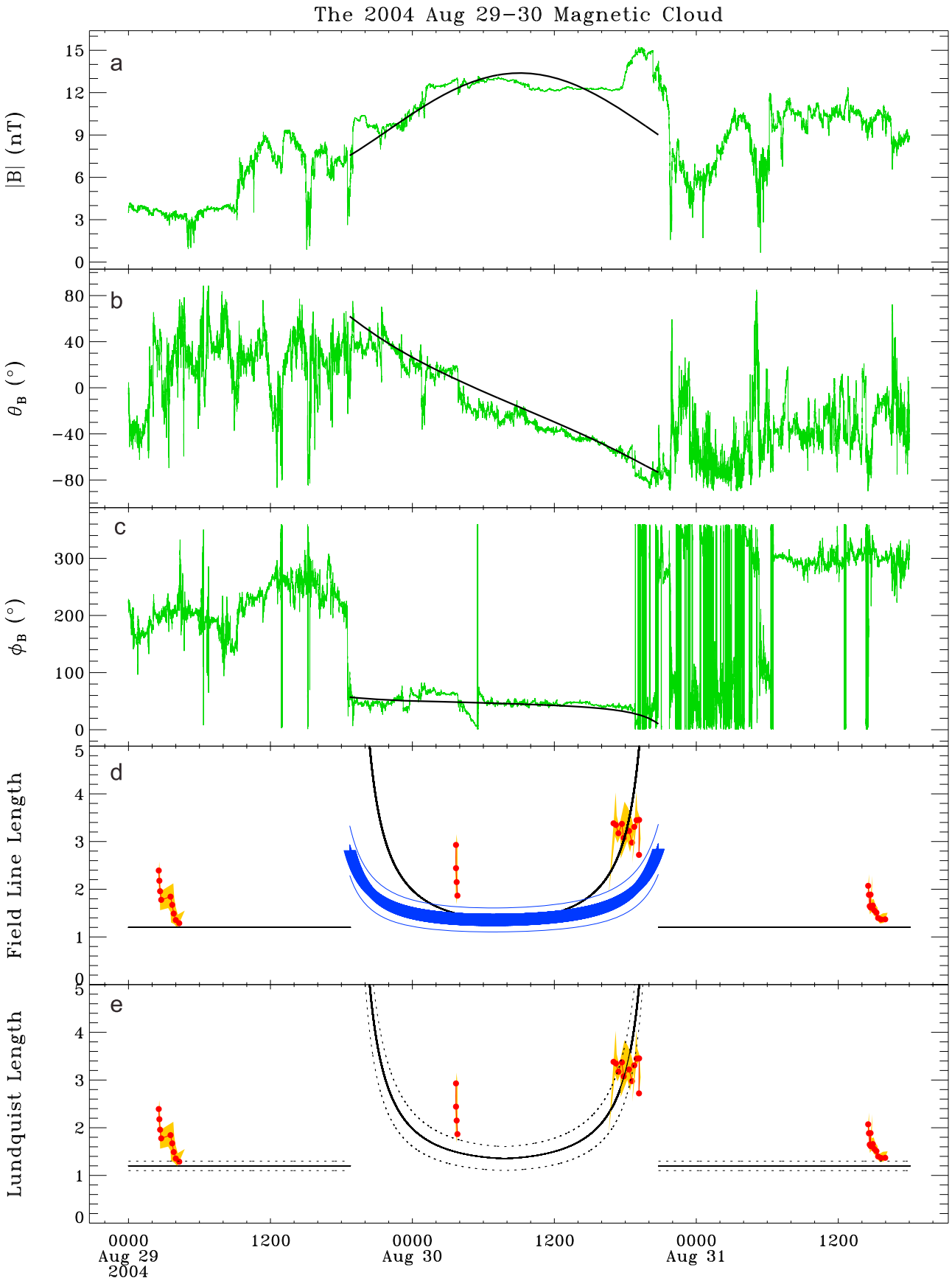

Figure 5. Same format as in Figure 4, but for MC 81.

Table 2. Comparison of MC Start and End Times With Other Work

MC	Onset Time (UT)	End Time (UT)	Reference[a]	Time Ranges and Notes[b]
6	18 Oct 1995 19.8	20 Oct 1995 01.3	MFI	1, 0 h
	18 Oct 1995 19.0	20 Oct 1995 01.6	L97	
	18 Oct 1995 19.0	20 Oct 1995 01.6	J06	
21	18 Sep 1997 00.5	20 Sep 1997 12.5	MFI	3, 9 h
	18 Sep 1997 03.0	19 Sep 1997 21.0	H05	18 Sep 1997, 20 events outside MC
	no listing	no listing	CRC03	
	18 Sep 1997 04.0	20 Sep 1997 12.0	J06	18 Sep 1997 event outside MC
32	2 May 1998 12.3	3 May 1998 17.3	MFI	8, 5 h
	2 May 1998 13.0	3 May 1998 12.0	S99	
	2 May 1998 12.0	3 May 1998 17.0	H05	
	2 May 1998 05.0	3 May 1998 17.0	CR03	
	2 May 1998 09.0	3 May 1998 17.0	J06	
54	6 Nov 2000 23.1	7 Nov 2000 18.1	MFI	1, 12 h
	6 Nov 2000 22.0	7 Nov 2000 15.0	H05	7 Nov 2000 event just outside MC
	6 Nov 2000 22.0	7 Nov 2000 18.0	CR03	
	6 Nov 2000 22.5	8 Nov 2000 03.4	J06	7 Nov 2000 events (3) outside MC
61	10 Jul 2001 17.3	12 Jul 2001 08.8	MFI	38, 10 h
	10 Jul 2001 17.0	11 Jul 2001 23.0	H05	12 Jul 2001 event outside MC
	10 Jul 2001 17.0	12 Jul 2001 09.0	CR03	
	9 Jul 2001 03.0	12 Jul 2001 03.0	J06	
72.2	30 Sep 2002 22.6	1 Oct 2002 11.9	MFI	1, 3 h
	30 Sep 2002 23.0	1 Oct 2002 15.0	H05	
	30 Sep 2002 22.0	1 Oct 2002 13.0	CR03	
	30 Sep 2002 22.0	1 Oct 2002 14.5	J06	
80	24 Jul 2004 12.8	25 Jul 2004 13.3	MFI	2, 2 h
	24 Jul 2004 14.0	25 Jul 2004 15.0	CR03	25 Jul 2004 event inside MC
	24 Jul 2004 12.1	25 Jul 2004 15.6	J06	25 Jul 2004 event inside MC
81	29 Aug 2004 18.7	30 Aug 2004 20.8	MFI	10, 2 h
	29 Aug 2004 19.0	30 Aug 2004 22.0	CR03	
	29 Aug 2004 09.1	30 Aug 2004 20.3	J06	

[a]MFI [*Lepping et al.*, 2006], L97 [*Larson et al.*, 1997], S99 [*Skoug et al.*, 1999], H05 [*Huttunen et al.*, 2005], CR03 [*Cane and Richardson*, 2003] (http://www.ssg.sr.unh.edu/mag ace/ACElists/ICMEtable.html), J06 [*Jian et al.*, 2006].
[b]Maximum differences in onset, end times in hours. Also, any displacements of electron event MC locations relative to the MFI onset and end times.

[*Larson et al.*, 1997]. The two models used here have revealed an important result that the definitive MC model tests with the particle data must be done in the outer regions of the MCs. The model MC field line lengths there are significantly longer than estimated Parker spiral lengths and thus provide good tests for the deduced path lengths only when $r/R_0 > 0.5$ (Figures 4 and 5). If we take a field line length of 4 AU as the lower limit for a definitive flux rope model test prediction, then this study was limited to 10 cases of the Lundquist model and 5 of the Flux Conservation model. However, there is little overlap between those model lengths and the $Le > 2.5$ AU points of Figures 4 and 5.

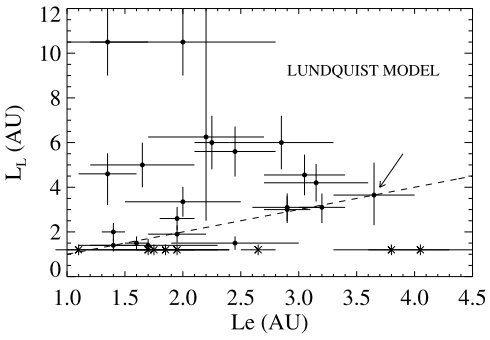

Figure 6. Plot of the field line lengths L_L versus the averaged electron event field line lengths Le for all events of Table 1. Solid dots are points inside the MCs, and crosses are points outside the MCs. Diagonal line marks $L_L = Le$.

[24] Figures 4 and 5 also show that calculated field line lengths near the MC boundaries are highly model dependent. The agreement between our two models appears best for MCs 6 and 54 and worst for MCs 21 (Figure 4) and 72.2. In MC 21 the L_{FC} field line lengths reached maximum well inside the boundaries of the MC at $r/R_0 = 0.6$ and then decreased toward the MC boundary. This same effect occurred for L_{FC} at the initial 18 October MC encounter in Figure 1, where MC parameters different from ours were used for that calculation [*Larson et al.*, 1997]. In contrast, the Lundquist model we used required that the longest L_L occurs at the MC boundary. This fundamental difference in model field line lengths at or near MC boundaries stands out when we consider the first and last events of MC 21 (Table 1), which occurred near the MC

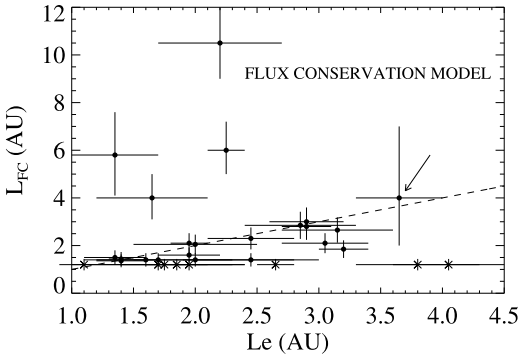

Figure 7. Same format as in Figure 7, but for L_{FC}.

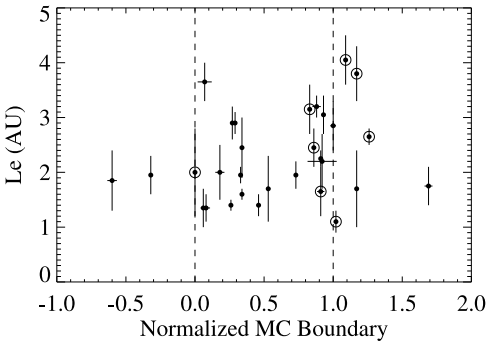

Figure 8. Superposed epoch plot of *Le* versus location relative to the boundaries of the eight MCs, indicated by the vertical dashed lines. The MC durations, taken from the Magnetic Cloud Table 2 web site and ranging from 13 to 60 h, are normalized to unity. Each data point represents one 3DP electron event of Table 1. This plot allows us to evaluate the implications of a flux rope interpretation independently of any flux rope model. The circled points are those which would be displaced across an MC boundary if alternative boundaries of Table 2 were used.

boundaries. The *Le* of those events are in good accord with L_{FC} but much smaller than the large L_L values.

4.2. Alternative MC Models and Effects

[25] Other models have been employed for MC flux rope fits. The same four different cylindrically symmetric flux rope models, two force-free and two non-force-free [*Russell and Mulligan*, 2003], were fitted to 20 MCs [*Gulisano et al.*, 2005] and to MC 6 [*Dasso et al.*, 2006] to calculate their magnetic helicities per unit length. The distribution of the magnetic axial twist per unit length, $\tau(r) = d\phi/dz$ is distributed differently in those models [*Dasso et al.*, 2006], which include the force-free Lundquist model we used. However, the fitted MC values of $\tau(0) \sim 5$–20 rad/AU for the four different models [*Gulisano et al.*, 2005] suggest that the models could have comparable distributions of field line lengths but with rather different radial distributions. A comparison of the two force-free models with a recent non-cylindrically symmetric flux rope model [*Krittinatham and Ruffolo*, 2009] supports that suggestion.

[26] Another effect not included here is the nonradial expansion of MC cross sections due to the diverging spherical geometry of the solar wind. *Riley and Crooker* [2004] modeled the expansion of an MC with a pressure gradient between the flux rope and the solar wind and found an MC aspect ratio (latitudinal to radial extents) of ~5 at 1 AU. Consideration of various solar wind environments has led to further MC models with bent and/or convex or concave oblate boundaries [*Owens*, 2006; *Démoulin and Dasso*, 2009]. The field line lengths in the outer parts of those MCs would be lengthened from those of the cylindrically symmetric models by factors of about the aspect ratios, but this does not apply to the quasi-radial field line segments closer to the Sun, which were not part of the expansion models. Thus we think that the basic results of our comparison of electron path lengths with the MC model field line lengths are not biased by the particular MC models used here.

[27] The azimuthal magnetic flux gives MCs their characteristic twisted flux-rope nature and provides the long path lengths optimal for testing the models with electron events. The azimuthal fields and field line lengths are most sensitive to model variations at the MC boundaries [*Démoulin*, 2008], and that is why the boundary locations are crucial for accurate modeling [*Riley et al.*, 2004], and efforts continue to refine the defining criteria [*Lepping et al.*, 2009]. We have compared in Table 2 the boundary locations of the eight MCs determined from several sources. The median boundary differences are only 2 to 4 h, but in the eight cases indicated in Figure 8 the other studies would switch the 3DP electron events from outside to inside the MC or vice versa. The MC boundary uncertainty is a concern, but it also does not invalidate our results.

4.3. Implications for the Flux Rope Interpretation

[28] With our limited number of data points in Figures 6 and 7 we also found no distinction of path lengths *Le* between the 22 calculated MC fields and their eight external fields, suggesting no difference in path length distributions between MCs and their surrounding solar wind fields. Even the assumption of a flux rope with longer field line lengths at the MC boundaries is not supported by the superposed epoch plot of Figure 8. In section 1.1 we reviewed some of the ambiguous or contradictory results obtained in efforts to explore the solar energetic particle signatures of fields in MCs or ICMEs. The lack of a clear difference in the calculated *Le* between MC interiors and exteriors constitutes another such example. One reason may be that a substantial amount of interchange reconnection has taken place between the outer fields of some MCs and the surrounding solar wind fields [*Larson et al.*, 1997; *Dasso et al.*, 2006; *Baker et al.*, 2009], providing direct magnetic connections to the Sun through field lines exterior to the MCs. Reconnection occurring across current sheets formed within oblate MCs [*Gosling and Szabo*, 2008; *Owens*, 2009] could also diminish the initial extended field line lengths in the outer regions of those MCs. A recent approach has considered poloidal flux conservation between MCs and their associated photospheric active regions to find axial lengths of MCs carrying the magnetic twist. *Yamamoto et al.* [2010] found MC poloidal lengths of only 0.01 to 1.25 AU, contrary to the usual assumption that the poloidal lengths extend to 2.5 AU or greater. That would generally imply substantially shorter model field line lengths than we calculated here, especially at the MC boundaries.

[29] The similarity of the interior and exterior MC *Le* values may also be consistent with recent modeling showing that the field rotations characteristic of MCs may not be flux ropes at all but rather the writhe of the magnetic fields produced by lower coronal reconnection between the erupting field and the global field [*Jacobs et al.*, 2009]. Alternatively, simulations of single reconnection events in current sheets with guide fields have shown that the reconnected fields can sweep up unreconnected guide fields, creating a field rotation looking like a flux rope twist [*Linton and Moldwin*, 2009]. Lacking the high twist of flux ropes, the field line lengths in such cases would probably be much shorter than expected for flux ropes and more in accord with our results of a lack of clear difference between interior and exterior field line lengths of MCs.

[30] Our goal here has been to test specific MC models by their calculated field line lengths. We expected that if significant twist is characteristic of MC models in general, we should have found some cases of large *Le* in the MC outer regions. A possible extension of this work is to test flux rope models for MCs at distances beyond 1 AU, for which the field line lengths are much longer than at 1 AU. Calculating path lengths for electrons in all ICMEs, not only MCs, could explore differences in field geometries between MCs and non-MCs. In the absence of any geometric model we can still ask whether we find evidence in any ICMEs for the presence of extended $Le > 4$ AU electron path lengths, which could indicate the presence of twisted flux ropes in those ICMEs.

[31] **Acknowledgments.** We acknowledge the Wind MFI and 3DP instrument teams for the use of their data. The work at UC Berkeley was supported through NASA grant NNG 05GH18G for Wind. The work at AFRL was supported by AFOSR work unit 2301RDZ4. The work benefited considerably from comments of the reviewers and of colleagues at Caltech.

[32] Philippa Browning thanks Olga Malandraki and another reviewer for their assistance in evaluating this paper.

References

Baker, D., et al. (2009), Signatures of interchange reconnection: STEREO, ACE and Hinode observations combined, *Ann. Geophys.*, *27*, 3883–3897.

Burlaga, L. F. (1995), *Interplanetary Dynamics*, Oxford Univ. Press, New York.

Burlaga, L. F., R. P. Lepping, and J. A. Jones (1990), Global configuration of a magnetic cloud, in *Physics of Magnetic Flux Ropes*, *Geophys. Monogr. Ser.*, vol. 58, edited by C. T. Russell, E. R. Priest, and L. C. Lee, pp. 373–377, AGU, Washington, D. C.

Cane, H. V., and I. G. Richardson (2003), Interplanetary coronal mass ejections in the near-Earth solar wind during 1996–2002, *J. Geophys. Res.*, *108*(A4), 1156, doi:10.1029/2002JA009817.

Crooker, N. U., J. T. Gosling, and S. W. Kahler (2002), Reducing heliospheric magnetic flux from coronal mass ejections without disconnection, *J. Geophys. Res.*, *107*(A2), 1028, doi:10.1029/2001JA000236.

Dasso, S., C. H. Mandrini, P. Démoulin, and M. L. Luoni (2006), A new model-independent method to compute magnetic helicity in magnetic clouds, *Astron. Astrophys.*, *455*, 349–359.

Démoulin, P. (2008), A review of the quantitative links between CMEs and magnetic clouds, *Ann. Geophys.*, *26*, 3113–3125.

Démoulin, P., and S. Dasso (2009), Magnetic cloud models with bent and oblate cross-section boundaries, *Astron. Astrophys.*, *507*, 969–980.

Farrugia, C. J., I. G. Richardson, L. F. Burlaga, R. P. Lepping, and V. A. Osherovich (1993), Simultaneous observations of solar MeV particles in a magnetic cloud and in the earth's northern tail lobe: Implications for the global field line topology of magnetic clouds and for the entry of solar particles into the magnetosphere during cloud passage, *J. Geophys. Res.*, *98*, 15,497–15,507.

Feuerstein, W. M., D. E. Larson, J. G. Luhmann, R. P. Lin, S. W. Kahler, and N. U. Crooker (2004), Parameters of solar wind electron heat-flux pitch-angle distributions and IMF topologies, *Geophys. Res. Lett.*, *31*, L22805, doi:10.1029/2004GL020529.

Forbes, T. G., et al. (2006), Theory and models: Report of working group D, *Space Sci. Rev.*, *123*, 251–302.

Gosling, J. T., and A. Szabo (2008), Bifurcated current sheets produced by magnetic reconnection in the solar wind, *J. Geophys. Res.*, *113*, A10103, doi:10.1029/2008JA013473.

Gulisano, A. M., S. Dasso, C. H. Mandrini, and P. Démoulin (2005), Magnetic clouds: a statistical study of magnetic helicity, *J. Atmos. Sol. Terr. Phys.*, *67*, 1761–1766.

Haggerty, D. K., and E. C. Roelof (2002), Impulsive near-relativistic solar electron events: Delayed injection with respect to solar electromagnetic emission, *Astrophys. J.*, *579*, 841–853.

Haggerty, D. K., E. C. Roelof, and G. M. Simnett (2003), Escaping near-relativistic electron beams from the solar corona, *Adv. Space Res.*, *32*, 2673–2678.

Huttunen, K. E. J., R. Schwenn, V. Bothmer, and H. E. J. Koskinen (2005), Properties and geoeffectiveness of magnetic clouds in the rising, maximum and early declining phases of solar cycle 23, *Ann. Geophys.*, *23*, 625–641.

Jacobs, C., I. I. Roussev, N. Lugaz, and S. Poedts (2009), The internal structure of coronal mass ejections: are all regular magnetic clouds flux ropes?, *Astrophys. J.*, *695*, L171–L175.

Jian, L., C. T. Russell, J. G. Luhmann, and R. M. Skoug (2006), Properties of interplanetary coronal mass ejections at one AU during 1995–2004, *Sol. Phys.*, *239*, 393–436.

Kahler, S. W. (2007), Solar sources of heliospheric energetic electron events – Shocks or flares?, *Space Sci. Rev.*, *129*, 359–390.

Kahler, S. W., and B. R. Ragot (2006), Near-relativistic electron c/v onset plots, *Astrophys. J.*, *646*, 634–641.

Kahler, S., S. Krucker, and A. Szabo (2009), Energetic electron probes of magnetic cloud topology, *Conf. Pap. Int. Cosmic Ray Conf. 31st*, in press.

Kilpua, E. K. J., et al. (2009), Multispacecraft observations of magnetic clouds and their solar origins between 19 and 23 May 2007, *Sol. Phys.*, *254*, 325–344.

Krittinatham, W., and D. Ruffolo (2009), Drift orbits of energetic particles in an interplanetary magnetic flux rope, *Astrophys. J.*, *704*, 831–841.

Krucker, S., D. E. Larson, R. P. Lin, and B. J. Thompson (1999), On the origin of impulsive electron events observed at 1 AU, *Astrophys. J.*, *519*, 864–875.

Larson, D. E., et al. (1997), Tracing the topology of the October 18–20, 1995, magnetic cloud with ~0.1–10^2 keV electrons, *Geophys. Res. Lett.*, *24*, 1911–1914.

Lepping, R. P., L. F. Burlaga, and J. A. Jones (1990), Magnetic field structure of interplanetary magnetic clouds at 1 AU, *J. Geophys. Res.*, *95*, 11,957–11,965.

Lepping, R. P., et al. (1995), The WIND Magnetic Field Investigation, *Space Sci. Rev.*, *71*, 207–229.

Lepping, R. P., D. B. Berdichevsky, and T. J. Ferguson (2003), Estimated errors in magnetic cloud model fit paramters with force-free cylindrically symmetric asumptions, *J. Geophys. Res.*, *108*(A10), 1356, doi:10.1029/2002JA009657. (Correction, *J. Geophys. Res., 109*, A07101, doi:10.1029/2004JA010517.)

Lepping, R. P., D. B. Berdichevsky, C.-C. Wu, A. Szabo, T. Narock, F. Mariani, A. J. Lazarus, and A. J. Quivers (2006), A summary of WIND magnetic clouds for years 1995–2003: Model-fitted parameters, associated errors and classifications, *Ann. Geophys.*, *24*, 215–245.

Lepping, R. P., T. W. Narock, and C.-C. Wu (2009), A scheme for finding the front boundary of an interplanetary magnetic cloud, *Ann. Geophys.*, *27*, 1295–1311.

Lin, R. P., et al. (2008), The STEREO IMPACT Suprathermal Electron (STE) instrument, *Space Sci. Rev.*, *136*, 241–255.

Linton, M. G., and M. B. Moldwin (2009), A comparison of the formation and evolution of magnetic flux ropes in solar coronal mass ejections and magnetotail plasmoids, *J. Geophys. Res.*, *114*, A00B09, doi:10.1029/2008JA013660.

Liu, Y., J. G. Luhmann, K. E. J. Huttunen, R. P. Lin, S. D. Bale, C. T. Russell, and A. B. Galvin (2008), Reconstruction of the 2007 May 22 magnetic cloud: How much can we trust the flux-rope geometry of CMEs?, *Astrophys. J.*, *677*, L133–L136.

Luhmann, J. G., et al. (2008), STEREO IMPACT investigation goals, measurements, and data products overview, *Space Sci. Rev.*, *136*, 117–184.

Malandraki, O., E. T. Sarris, and P. Trochoutsos (2000), Probing the magnetic topology of coronal mass ejection by means of Ulysses/HI-SCALE energetic particle observations, *Ann. Geophys.*, *18*, 129—140.

Malandraki, O. E., E. T. Sarris, L. J. Lanzerotti, C. G. Maclennan, M. Pick, and G. Tsiropoula (2001), Tracing the magnetic topology of coronal mass ejection events by ULYSSES/HI-SCALE energetic particle observations in and out of the ecliptic, *Space Sci. Rev.*, *97*, 129–140.

Malandraki, O., D. Lario, L. J. Lanzerotti, E. T. Sarris, A. Geranios, and G. Tsiropoula (2005), October/November 2003 interplanetary coronal mass ejections: ACE/EPAM solar energetic particle observations, *J. Geophys. Res.*, *110*, A09S06, doi:10.1029/2004JA010926.

Owens, M. J. (2006), Magnetic cloud distortion resulting from propagation through a structured solar wind: Models and observations, *J. Geophys. Res.*, *111*, A12109, doi:10.1029/2006JA011903.

Owens, M. J. (2009), The formation of large-scale current sheets with magnetic clouds, *Sol. Phys.*, *260*, 207–217.

Owens, M. J., N. U. Crooker, and T. S. Horbury (2009), The expected imprint of flux rope geometry on suprathermal electons in magnetic clouds, *Ann. Geophys.*, *27*, 4057–4067.

Ragot, B. R. (2006), Lengths of wandering magnetic field lines in the turbulent solar wind, *Astrophys. J.*, *653*, 1493–1498.

Ragot, B. R., and S. W. Kahler (2008), Travel delays of impulsive SEPs due to turbulent lengthening of magnetic field lines, *30th Int. Cosmic Ray Conf.*, *1*, 147–150.

Richardson, I. G. (1997), Using energetic particles to probe the magnetic topology of ejecta, in *Coronal Mass Ejections*, *Geophys. Monogr. Ser.*,

vol. 99, edited by N. Crooker, J. A. Joselyn, and J. Feynmann, pp. 189–196, AGU, Washington, D.C.

Richardson, I. G., and H. V. Cane (1996), Particle flows observed in ejecta during solar event onsets and their implication for the magnetic field topology, *J. Geophys. Res.*, *101*, 27,521–27,532.

Riley, P., and N. U. Crooker (2004), Kinematic treatment of coronal mass ejection evolution in the solar wind, *Astrophys. J.*, *600*, 1035–1042.

Riley, P., et al. (2004), Fitting flux ropes to a global MHD solution: a comparison of techniques, *J. Atmos. Sol. Terr. Phys.*, *66*, 1321–1331.

Russell, C. T., and T. Mulligan (2003), The limitation of Bessel functions for ICME modeling, in *Solar Wind Ten*, edited by M. Velli, R. Bruno, and F. Malara, *AIP Conf. Proc.*, *679*, 125–128.

Shodhan, S., N. U. Crooker, S. W. Kahler, R. J. Fitzenreiter, D. E. Larson, R. P. Lepping, G. L. Siscoe, and J. T. Gosling (2000), Counterstreaming electrons in magnetic clouds, *J. Geophys. Res.*, *105*, 27,261–27,268.

Skoug, R. M., et al. (1999), A prolonged He^{+} enhancement within a coronal mass ejection in the solar wind, *Geophys. Res. Let.*, *26*, 161–164.

Wimmer-Schweingruber, R., et al. (2006), Understanding interplanetary mass ejection signatures: Report of working group B, *Space Sci. Rev.*, *123*, 177–216.

Yamamoto, T. T., R. Kataoka, and S. Inoue (2010), Helical lengths of magnetic clouds from the magnetic flux conservation, *Astrophys. J.*, *710*, 456–461.

Zurbuchen, T. H., and I. G. Richardson (2006), In-situ solar wind and magnetic field signatures of interplanetary coronal mass ejections, *Space Sci. Rev.*, *123*, 31–43.

S. W. Kahler, Space Vehicles Directorate, Air Force Research Laboratory, 29 Randolph Rd., Hanscom AFB, MA 01731, USA. (AFRL.RVB.PA@hanscom.af.mil)

S. Krucker, Space Sciences Laboratory, University of California, 7 Gauss Way, Berkeley, CA 94720, USA.

A. Szabo, Heliospheric Physics Laboratory, NASA Goddard Space Flight Center, Greenbelt, MD 20771, USA.